Chinese Chemical Letters 37 (2026) 111274

Contents lists available at ScienceDirect

Chinese Chemical Letters

journal homepage: www.elsevier.com/locate/cclet

Tailoring anode properties with carbon nanofiber-interpenetrated graphene aerogels for high-performance bioelectrochemical systems

Tingli Ren[a], Yuanfeng Liu[a,b,*], Congju Li[a,c,*]

[a] School of Energy and Environmental Engineering, University of Science and Technology Beijing, Beijing 100083, China
[b] The Key Laboratory of Water and Sediment Sciences, Ministry of Education, College of Environment Sciences and Engineering, Peking University, Beijing 100871, China
[c] College of Textiles, Donghua University, Shanghai 201620, China

ARTICLE INFO

Article history:
Received 18 February 2025
Revised 25 April 2025
Accepted 28 April 2025
Available online 29 April 2025

Keywords:
Electroactive biofilm
Bioelectrochemical system
Power density
Carbon nanofibers
Graphene aerogel

ABSTRACT

The poor biofilm colonization, charge transfer, and storage at the anode have long been major obstacles to achieving high power generation in bioelectrochemical systems (BES). To overcome this challenge, we developed electrospun carbon nanofiber-interpenetrated reduced graphene oxide aerogels (CNF/rGO-x, where x denotes the mass ratio of CNF to rGO, with x = 2, 4, 6) to modify the surface of carbon cloth (CC), significantly enhancing its electrochemical performance. The CNF/rGO-6 aerogel featured a porous, interconnected conductive scaffold, endowing the CC electrode with a larger electrochemically active area, higher specific capacitance, and a rougher surface. These properties significantly improved biofilm adhesion, extracellular electron transfer, and charge storage capabilities. As a result, the BES equipped with a CNF/rGO-6 electrode achieved an impressive power density of 3080.3 mW/m^2, significantly higher than those of BES with CNF/rGO-4 (2426.3 mW/m^2), CNF/rGO-2 (2717 mW/m^2), rGO (1978.3 mW/m^2), and pure CC (1050.4 mW/m^2) electrodes. Furthermore, the CNF/rGO-6 electrode supported a high abundance of electroactive bacteria and enhanced their viability. With its simple fabrication, low weight, and exceptional electrochemical performance, the CNF/rGO-6 aerogel demonstrates significant potential as an electrode material for high-performance and cost-effective BES.

© 2026 Published by Elsevier B.V. on behalf of Chinese Chemical Society and Institute of Materia Medica, Chinese Academy of Medical Sciences.

Bioelectrochemical systems (BESs) have garnered significant attention as sustainable technologies due to their dual capabilities in energy generation and wastewater treatment [1]. With increasing research efforts in this technology, BESs have demonstrated considerable potential in applications such as biosensors [2], electrical generators [3], and wastewater treatment [4]. However, the practical implementation of BES confronts major challenges, primarily stemming from limited power density, which is closely associated with poor biofilm colonization, sluggish extracellular electron transfer (EET), and inefficient charge storage at the anode interface. Improving the performance of electrode materials, which function as both current collectors and carriers for electroactive biofilm colonization, is essential for enhancing the electricity generation capabilities of BES [5,6]. Previous research has demonstrated that electrode materials with larger specific surface areas, higher electrical conductivity, and abundant porosity, capable of accommodating living bacterial cells, can significantly improve the overall performance of BES [7].

Traditional carbon-based materials, such as carbon cloth (CC), carbon paper and graphite sheets, are commonly used as electrode materials in BES due to their high mechanical strength and suitable chemical stability [8–10]. However, the performance of BESs employing these carbon-based electrodes remains suboptimal, primarily due to their limited porosity and inferior electrochemical characteristics that constrain both biofilm colonization and EET efficiency. To address these challenges, considerable efforts have been made to modify the surface properties of electrodes, by integrating materials like graphene [11], carbon nanotubes [12], conductive polymers [13] or transition metal oxides [14] onto the carbon supports. Among these, graphene has gained substantial attention as high-performance anode electrocatalyst for BES because of its large specific surface area, favorable biocompatibility, and exceptional electrical conductivity [15–17]. For instance, Liu *et al.* [18] demonstrated that reduced graphene oxide (rGO) as biocompatible electrode greatly enhanced biofilm adhesion, cell viability and EET activity at its interface. Similarly, Kirubaharan *et al.* [13] reported that rGO/polypyrrole hydrogels electrodes

* Corresponding authors.
E-mail addresses: liuyuanfeng1113@126.com (Y. Liu), congjuli@126.com (C. Li).

https://doi.org/10.1016/j.cclet.2025.111274
1001-8417/© 2026 Published by Elsevier B.V. on behalf of Chinese Chemical Society and Institute of Materia Medica, Chinese Academy of Medical Sciences.

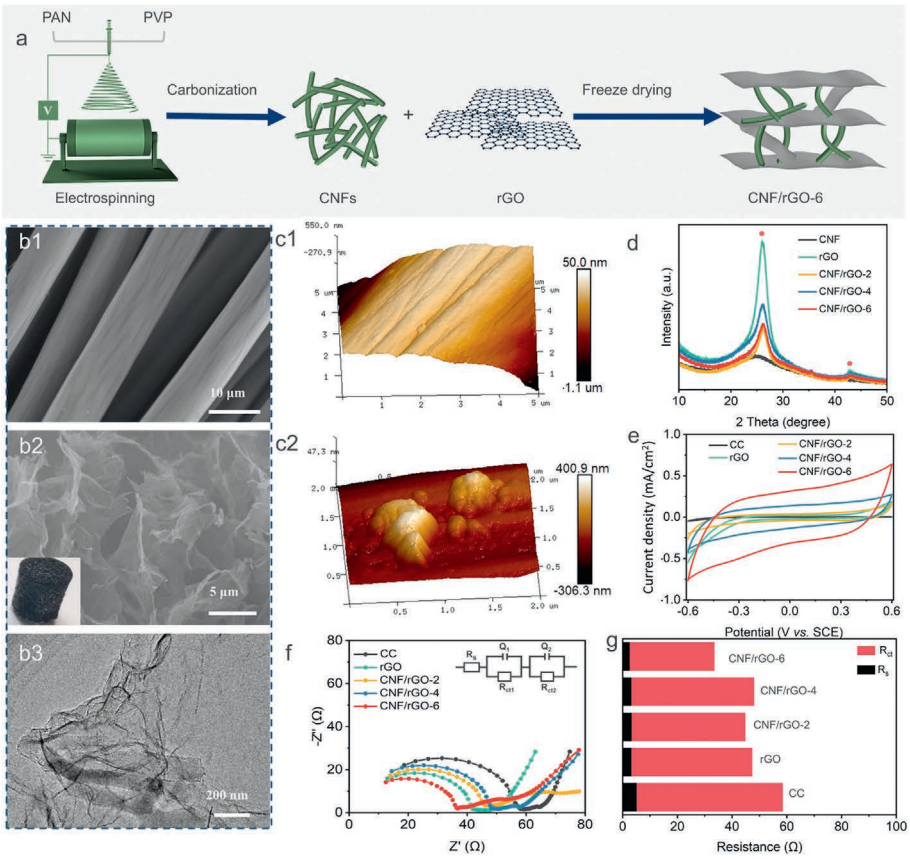


Fig. 1. (a) Schematic illustration of the fabrication process of the CNF/rGO-6 aerogel. SEM images of (b1) CC, (b2) CNF/rGO-6. (b3) TEM images of CNF/rGO-6. AFM images of (c1) CC, (c2) CNF/rGO-6. (d) The XRD patterns of all as-prepared samples. (e) The CV curves, (f) Nyquist curves and (g) the fitted values of R_{ohm} and R_{ct} of different electrodes.

achieved an 8.6-fold increase in power density compared to bare electrodes. However, the application of pristine rGO electrodes remains limited by inherent material challenges, including nanosheet agglomeration, and restricted pore size, which negatively impact bacterial adhesion and ultimately limit power generation efficiency in BES. The construction of three-dimensional aerogel architectures through the incorporation of conductive pillars as structural supports represents a promising strategy to overcome these limitations by preventing rGO nanosheet aggregation and creating continuous conductive networks, thereby enhancing both bacterial loading capacity and electrochemical activity [19].

Herein, we present the fabrication of three-dimensional porous aerogels composed of conductive carbon nanofibers (CNFs) interspersed with rGO nanosheets (CNF/rGO), through the electrospinning, carbonization and freeze-drying processes. This design was based on the following considerations: (i) Electrospun CNF establish a continuous electron transfer pathway between rGO nanosheets, facilitating charge transfer between the electroactive biofilm and the electrode [20]; (ii) CNFs serve as supporting pillars within the rGO framework, providing the hybrid materials with a stable porous architecture that can enhance the bacterial-cell accessibility and attachment onto the electrode; (iii) the porous structure can store electron shuttles (such as flavins [21], 2-amino-3-carboxy-1,4-naphthoquinone [22]), which mediate electron transfer from bacterial cells to the electrode, improving long-distance charge transfer. In this study, we investigated the mass ratio between CNF and rGO to analyze their morphologies and properties. The BES performance was evaluated using the as-synthesized electrodes, examining metrics such as power density, redox behavior, and charge transfer. Additionally, the biofilm characteristics—such as morphology, community composition and viability—on different electrodes were assessed. Finally, based on the characterizations and experimental results, we discuss the potential mechanisms behind the enhanced EET activity and BES performance facilitated by the CNF/rGO aerogels.

Fig. 1a illustrates the fabrication process of the CNF/rGO-x aerogels, where x denotes the mass ratio of CNF to rGO. In detail, CNFs prepared by electrospinning and carbonization were cut into shorter fibers using a high-speed homogenizer, and dissolved in rGO solutions. Then, the CNF/rGO-x aerogels were obtained *via* a freeze-drying process. The surface morphology and roughness of the prepared materials are examined using scanning electron microscope (SEM), transmission electron microscope (TEM) and atomic force microscope (AFM). As shown in Fig. 1b1, pure CC exhibits a cross-linked structure with a relatively smooth fiber surface (Figs. 1b1 and c1). In contrast, the CNF/rGO-6 aerogel displays a multilayered porous structure (Figs. 1b2, 1b3 and 1c2), indicating superior specific surface area and roughness compared to the other prepared aerogels (Fig. S1 in Supporting information). One-dimensional CNFs act as structural pillars, forming a mechanically interlocked three-dimensional skeleton network between the two-dimensional rGO layers. This unique architecture effectively prevents the restacking and agglomeration of rGO nanosheets induced by van der Waals forces interactions [23]. By physically separating and anchoring the rGO nanosheets, the CNFs simultaneously create and maintain a highly porous structure in the CNF/rGO-6 aerogel. It is well established that a high degree of porosity in electrodes enhances specific capacitance and charge storage, both crucial for improving electrode performance [24]. The X-ray diffractometer (XRD) patterns of the samples exhibit consistent broad

peaks around 26° and small peaks near 43°, corresponding to the (004) and (100) planes of graphitic carbon (PDF#26-1080), as shown in Fig. 1d [25]. The graphitization degree and defect level of the prepared samples can be assessed by the intensity ratio of the D and G peak (I_D/I_G) in the Raman spectra [26]. As shown in Fig. S2 (Supporting information), the broad peaks at approximately 1343 and 1589 cm^{-1} correspond to the D and G bands, respectively. The I_D/I_G ratio of CNF/rGO-6 is calculated to be 1.18, which is higher than that of CNF/rGO-2 (1.16) and CNF/rGO-4 (1.17), implying that the electrocatalytic activity of CNF/rGO-6 is significantly enhanced by increasing the CNF ratio. The X-ray photoelectron spectroscopy (XPS) spectrum, which included the C 1s, N 1s and O 1s characteristic peaks, is shown in Figs. S3a–c (Supporting information). Specifically, the high-resolution C 1s spectrum is deconvoluted into four distinct peaks at 284.9, 285.4, 286.4 and 289.2 eV, corresponding to the C=C, C-N, C=N/C=O and O=C=O bonding sites, respectively [27,28]. These chemical compositions are verified by Fourier transform infrared spectroscopy (FTIR, Fig. S3d in Supporting information). The formation of *N*-containing and *O*-containing groups can be attributed to the pyrolysis of the polymer and the formation of graphitic carbon, which facilitates enhanced charge transfer at the electrode interface [29]. The high-resolution N 1s spectrum exhibits four peaks, where the peaks at 397.8, 399.8, 400.9, and 405.8 eV are assigned to pyridinic N, pyrrolic N, graphitic N, and oxidized N, respectively [30–32]. Notably, pyrrolic N and graphitic N incorporated into the carbon lattice can effectively promote electron harvesting from the outer membrane C-type cytochromes (c-cyts) on bacterial cells [33,34]. Based on these findings, it can be speculated that the CNF/rGO-6 aerogel, with its higher pyrrolic N and graphitic N contents, wound exhibit excellent EET efficiency, thereby improving BES performance.

The electrochemical performance of different electrodes is evaluated using cyclic voltammetry (CV) and electrochemical impedance spectroscopy (EIS) measurements. As shown in Fig. 1e and Fig. S4 (Supporting information), the pristine CC electrode displays a negligible current response over a wide potential range. After modification with aerogel, the corresponding electrodes exhibit enhanced current responses and larger loop closure areas, owing to the increased interfacial porosity. Notably, the CNF/rGO-6 electrode presents the strongest current response and the largest loop closure area. Its specific capacitance is calculated to be 14.1 mF/cm^2, significantly higher than those of the pristine CC, rGO, CNF/rGO-2, and CNF/rGO-4 electrodes (Fig. S5 in Supporting information), implying its superior charge storage capacity [35]. The Nyquist plots of the electrodes are shown in Fig. 1f, with an inset displaying the equivalent circuit. The semicircle in the high-frequency region corresponds to the charge transfer resistance (R_{ct}), while the straight line in the low-frequency region represents the Warburg diffusion, which reflects ion diffusion ability. All electrodes exhibit similar ohmic resistance (2.7–5.2 Ω), which is attributed to the shared current collectors. However, the R_{ct} values varies significantly due to differences in interfacial properties, with the CNF/rGO-6 electrode exhibiting the lowest R_{ct} of 38.4 Ω, suggesting enhanced charge transfer efficiency (Fig. 1g). Based on the above results, it can be concluded that the CNF/rGO-6 electrode demonstrated superior charge storage capacity and charge transfer efficiency, both of which are crucial for enhancing BES performance.

To further confirm the superior performance of the CNF/rGO-6 aerogel, its BES performance is evaluated. As shown in Fig. 2a, the CNF/rGO-6 electrode exhibits a current density of 9.11 A/m^2 under stable biofilm formation, significantly higher than the CNF/rGO-4 (8.32 A/m^2), CNF/rGO-2 (6.27 A/m^2), rGO (5.82 A/m^2) and CC (2.25 A/m^2) electrodes. Additionally, as the current density increased, the CNF/rGO-6 electrode demonstrates a gradual decline in voltage but maintains the highest voltage values at the same current density (Fig. 2b). Moreover, the BES equipped with the CNF/rGO-6

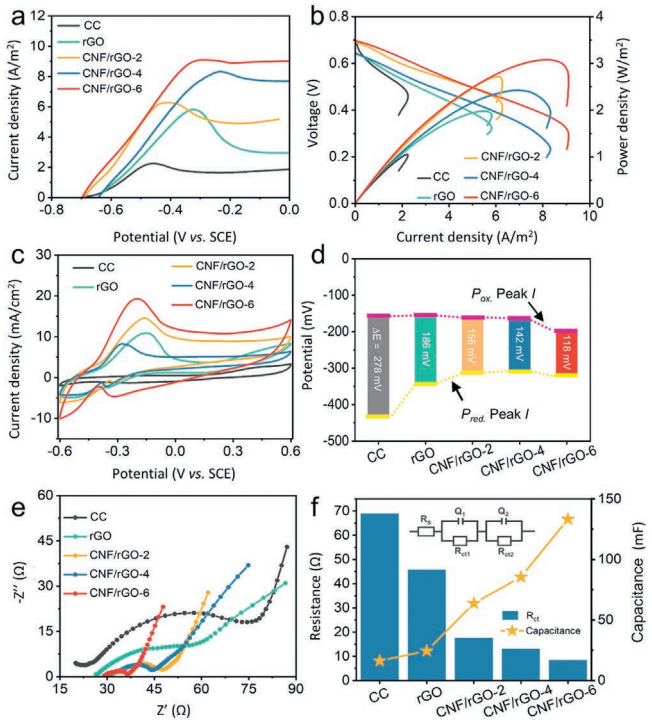


Fig. 2. (a) LSV curves, (b) power density and polarization curves, (c) CV curves, (d) redox potential difference, (e) Nyquist curves, (f) the fitted values of R_{ct} and corresponding capacitance of BESs equipped with different electrodes.

electrode achieves a maximum power density of 3080.3 mW/m^2, which is 2.9 times higher than that of the BES with the pure CC (1050.4 mW/m^2) electrode. In comparison to previously reported graphene aerogel-based anodes, the power density of the BESs with CNF/rGO-6 electrodes still demonstrates superior performance, as shown in Fig. S6 (Supporting information) [26,36–38]. The large specific surface area, porous structure, and high specific capacitance of CNF/rGO-6 aerogel enhance biofilm adhesion, charge storage, and EET activity, which significantly improve BES performance. Furthermore, the preparation of electrospun nanofibers is simple and cost-effective, making large-scale production more feasible compared to other polymeric materials. In view of the CV curves in Fig. 2c, all electrodes exhibit multiple pairs of redox peaks after stable biofilm formation, corresponding to redox reactions of biofilms with nutrients [39]. The redox peak pair of the BES with CNF/rGO-6 electrode at −200/−321 mV (centered at −261 mV) could be associated with OmcA (outer membrane c-type cytochrome) of the bacterial cells, suggesting the formation of dense biofilms with electrochemical activity [40,41]. Furthermore, the CNF/rGO-6 electrode exhibits the lowest redox potential separation of 118 mV compared to the other electrodes as shown in Fig. 2d, indicating its ability to easily accept and release electrons across the electrode [42]. This conclusion is further supported by the significantly reduced R_{ct} of 7.38 Ω of the BES equipped with the CNF/rGO-6 electrode as shown in Fig. 2e. Next, the capacitance of the electrodes is calculated from the EIS measurements, as shown in Fig. 2f. The CNF/rGO-6 electrode exhibits the highest capacitance of 133.25 mF, suggesting that even if the EET activity between the biofilm and electrode is hindered, the CNF/rGO-6 electrode can still function as an ideal charge reservoir for high power output [43,44]. The chemical oxygen demand (COD) removal efficiency, which indicated the ability of the BESs in treating the organic matter and reflected the properties of the biofilm on the c electrode, is demonstrated in Fig. S7 (Supporting information). In line with the results above, the BES with CNF/rGO-6 electrode

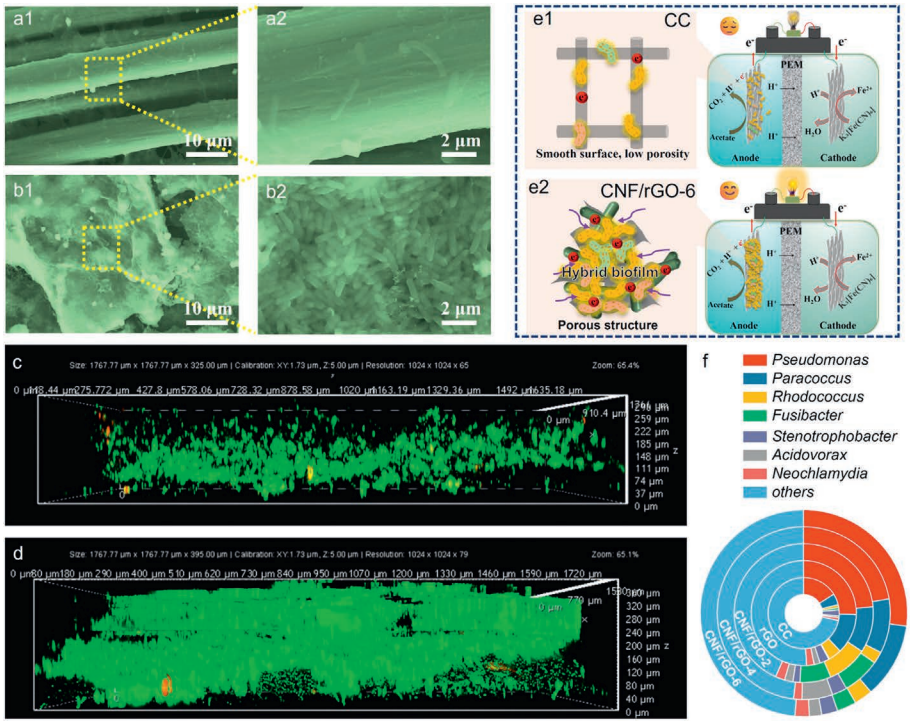


Fig. 3. SEM images of the biofilms on (a1, a2) CC, (b1, b2) CNF/rGO-6 electrode. CLSM images of the biofilms on (c) CC, (d) CNF/rGO-6 electrode. Potential mechanism for BESs with (e1) CC, (e2) CNF/rGO-6 electrode. (f) microbial community structure of different electrode samples at the genus level.

achieves the highest COD removal efficiency of 80.1 % ± 0.6 %, outperforming the BESs assembled with other electrodes, further confirming the superior biofilm activity on the CNF/rGO-6 electrode.

The morphology and viability of the biofilm on different electrodes are directly characterized using SEM and confocal scanning laser microscopy (CLSM), where the green fluorescent dots represent the surviving cells [45]. As shown in Figs. 3a1 and a2, only a few bacterial cells adhere to the pure CC electrode due to its planar structure and small-porosity. However, after modification with aerogels, the biofilm coverage on the electrode surface significantly increases (Figs. 3b1 and b2, Fig. S9 in Supporting information), attributed to the rough surface and enhanced porosity. Notably, the electrode modified with two-dimensional rGO nanosheets only alters its surface properties without addressing its internal structure, preventing full utilization of the potential internal surface area. Moreover, several studies have shown that dead bacteria and bacterial metabolites tend to accumulate on the surface of the two-dimensional structures during long-term BES operation [46]. This accumulation obstructs the channels for electron transfer and nutrient diffusion on the electrode, thereby reducing BES performance. The modification of electrode with CNF/rGO-x aerogels, which fully utilizes the internal space of electrode, proves to be an effective strategy. Consequently, continuous and dense biofilms adhere not only to the surface, but also to the internal pores of the electrode with CNF/rGO-x (Fig. 3d and Fig. S10 in Supporting information), due to its improved specific surface area, porosity, and bioaffinity. In contrast, the biofilm on the pristine CC electrode is sparse and discontinuous in two-dimensional space, as shown in Fig. 3c. Since proteins are crucial components of various enzymes and transporter proteins involved in cellular metabolic activities, a lower protein content on the CC electrode indicates slow biofilm growth, while a higher protein content on the CNF/rGO-6 electrode signifies active biofilm development (Fig. S11 in Supporting information) [47].

The bacterial community structure of the biofilm on the electrodes is identified through high-throughput 16S rRNA gene sequencing. The diversity and abundance index for different electrode samples are presented in Table S2 (Supporting information). All biofilm samples show similar coverage exceeding 0.99, indicating that all operational taxonomic units (OTUs) are detected and that the results accurately reflect the actual community structure of the samples. The relatively low Shannon index and high Simpson index for the biofilm on CNF/rGO-6 electrode suggest a decrease in microbial community diversity and an increase in uniformity, respectively [48]. Additionally, the high abundance-based coverage estimator (ACE) index indicates a selective enrichment effect of CNF/rGO-6 towards certain bacteria on the electrode. As shown in Figs. S12 and S13 (Supporting information), the abundance of predominant phylum varies slightly across different electrode samples. *Proteobacteria*, *Chloroflexi*, and *Actinobacteriota* are the common electroactive species, all of which are associated with enhanced power production in BESs [49]. The relative abundance of these electroactive species on the CNF/rGO-6 electrode is 70.1 %, which is higher than that on the other electrodes, furthermore confirming the selective enrichment of electrochemically active bacteria by CNF/rGO-6. At the genus level, the predominant bacterial genera include *Pseudomonas*, *Paracoccus*, and *Rhodococcus* (Fig. 3f). *Pseudomonas* has been shown to possess excellent electricity-producing capabilities using pollutants [50], while *Paracoccus* is a nitrifying bacterium capable of degrading pollutants [51]. *Rhodococcus* is one of the best-known electrogenic species in BESs [52]. The biofilms composed of electroactive and pollutant-degrading bacteria are selectively anchored on the electrode, contributing significantly to the enhanced power production performance and COD removal efficiency of the BESs, thanks to the electrode modification with a tailored structure.

In summary, we have developed a three-dimensional aerogel composed of CNFs interpenetrated with rGO nanosheets as a highly efficient electrode material for BESs. The BESs equipped with CNF/rGO-6 electrode exhibits a maximum power density of 3080.3 mW/m^2, which is 2.9 times higher than that of the pristine CC electrode. This enhancement can be attributed to the follow-

ing factors: (i) The rGO nanosheets supported by CNFs form a stable three-dimensional porous structure, offering improved porosity and a rough surface that promote bacterial growth and facilitate the transfer of nutrients/electron shuttles. (ii) The interconnected electron transfer channels and abundant electrochemically active sites within the aerogels impart excellent electrochemical properties to the electrodes, including high charge storage and fast charge transfer, which greatly enhance the EET activity between the biofilm and the electrode. (iii) The selective enrichment effect of the CNF/rGO-6 electrode enables electrochemically active bacteria to adhere to the electrode, forming a continuous and dense biofilm (Figs. 3e1 and e2). The synthesis of porous CNF/rGO-6 aerogels not only offers an effective approach for developing high-performance BES anodes, but also offers a versatile platform for electrode design in other electrochemical systems, such as hydrogen fuel cell, microbial electrolysis cell and supercapacitors. While these CNF/rGO-6 aerogels demonstrate significant promise, future research should focus on evaluating their performance under more realistic wastewater conditions, as well as assessing their mechanical strength, long-term stability and environmental impact for practical BES applications.

Declaration of competing interest

The authors declare that they have no known competing financial interests or personal relationships that could have appeared to influence the work reported in this paper.

CRediT authorship contribution statement

Tingli Ren: Writing – review & editing, Writing – original draft, Validation, Software, Methodology, Investigation. **Yuanfeng Liu:** Writing – review & editing, Writing – original draft, Validation, Methodology, Investigation, Formal analysis, Data curation, Conceptualization. **Congju Li:** Visualization, Validation, Supervision, Resources, Project administration, Funding acquisition, Conceptualization.

Acknowledgments

This work is supported by the National Natural Science Foundation of China (NSFC, Nos. 52170019 and 52103070), the Fundamental Research Funds for the Central Universities (No. 06500100), the “Ten thousand plan”-National High-level Personnel of special support program, the Postdoctoral Fellowship Program of CPSF (No. GZC20240034) and the China Postdoctoral Science Foundation (No. 2023M740075).

Supplementary materials

Supplementary material associated with this article can be found, in the online version, at doi:10.1016/j.cclet.2025.111274.

References

[1] X. Wu, D. Sun, M. Li, et al., Chem. Eng. J. 487 (2024) 150634.
[2] M. Lai, J. Hong, X. Xu, et al., Sens. Actuators B: Chem. 422 (2025) 136614.
[3] C. Li, K. Omine, Z. Zhang, et al., Energy Convers. Manag. 279 (2023) 116771.
[4] A.A. Al-Abbas, Z.Z. Ismail, J. Environ. Manag. 369 (2024) 122353.
[5] H.Z. Hamdan, D.A. Salam, Environ. Chem. Lett. 21 (2023) 2761–2787.
[6] R.S. Chouhan, S. Gandhi, S.K. Verma, et al., Renew. Sustain. Energy Rev. 188 (2023) 113813.
[7] C. Hou, D. Yang, B. Liang, et al., Anal. Chem. 86 (2014) 6057–6063.
[8] M. Hu, Y. Lin, X. Li, et al., Electrochim. Acta 404 (2022) 139618.
[9] Y. Zhang, F. Gao, D. Wang, et al., Coord. Chem. Rev. 475 (2023) 214916.
[10] Y. Zhang, Z. Li, K. Zhang, et al., Appl. Surf. Sci. 590 (2022) 153102.
[11] L.O. Hirsch, B. Gandu, A. Chiliveru, et al., Microorganisms 12 (2024) 604.
[12] Y. Liu, Y. Sun, M. Zhang, et al., J. Colloid Interface Sci. 629 (2023) 970–979.
[13] C.J. Kirubaharan, J.W. Wang, S.Z. Abbas, et al., Chemosphere 326 (2023) 138413.
[14] T.L. Ren, Y.F. Liu, C.H. Shi, et al., J. Colloid Interface Sci. 643 (2023) 428–436.
[15] Y. Wang, L. Wu, K. Qu, et al., Carbon 228 (2024) 119429.
[16] M. Xu, L. Wu, M. Zhu, et al., Carbon 193 (2022) 242–257.
[17] X. Ji, X. Li, C. Wang, et al., Chin. Chem. Lett. 35 (2024) 109388.
[18] F. Liu, Y. Yang, M. Xu, et al., Mater. Today Energy 39 (2024) 101464.
[19] H. Wu, H. Tan, L. Chen, et al., Chin. Chem. Lett. 32 (2021) 2499–2502.
[20] K.I. Hadjiivanov, D.A. Panayotov, M.Y. Mihaylov, et al., Chem. Rev. 121 (2020) 1286–1424.
[21] T. Lin, W. Ding, L. Sun, et al., Nano Energy 50 (2018) 639–648.
[22] E. Mevers, L. Su, G. Pishchany, et al., eLife 8 (2019) e48054.
[23] H. Tian, J. Qin, D. Hou, et al., Angew. Chem. Int. Ed. 58 (2019) 10173–10178.
[24] B.A. Hemdan, D.A. Jadhav, A. Dutta, et al., J. Water Process Eng. 54 (2023) 104065.
[25] Y. Wang, Renew. Energy 232 (2024) 121109.
[26] S. Jin, Y. Feng, J. Jia, et al., Energy Environ. Mater. 6 (2023) e12373.
[27] X. Sun, X.S. Wu, Z.Z. Shi, et al., J. Power Sources 530 (2022) 231277.
[28] H.A. Bandal, A.A. Pawar, H. Kim, Electrochim. Acta 422 (2022) 140545.
[29] S. You, M. Ma, W. Wang, et al., Adv. Energy Mater. 7 (2017) 1601364.
[30] Y. Hu, J.O. Jensen, W. Zhang, et al., ChemSusChem 7 (2014) 2099–2103.
[31] L.B. Zong, X. Chen, S.M. Dou, et al., Chin. Chem. Lett. 32 (2021) 1121–1126.
[32] S. Xu, J. Chen, H. Peng, et al., Fuel 291 (2021) 120128.
[33] D. Jiang, H. Xie, H. Chen, et al., Int. J. Hydrogen Energy 47 (2022) 35458–35467.
[34] B. Kim, G. Baek, C. Kim, et al., ACS ES&T Eng. 4 (2024) 1520–1539.
[35] L. Zou, Y. Qiao, Z.Y. Wu, et al., Adv. Energy Mater. 6 (2015) 1501535.
[36] D. Guo, X. Wang, Q. Fu, et al., Chemosphere 363 (2024) 142858.
[37] S. Liu, Z. Li, D. Liang, et al., Chem. Eng. J. 473 (2023) 145443.
[38] T. Zhao, Z. Qiu, Y. Zhang, et al., J. Environ. Chem. Eng. 9 (2021) 105441.
[39] Y. Hubenova, E. Hubenova, B. Burdin, et al., Electrochim. Acta 312 (2019) 432–440.
[40] L. Chen, L. Jiang, L. Cheng, et al., Chemosphere 350 (2024) 141073.
[41] J. Wang, B. Li, S.P. Wang, et al., J. Clean. Prod. 341 (2022) 130725.
[42] B.S. Thapa, T. Kim, S. Pandit, et al., Bioresour. Technol. 347 (2022) 126579.
[43] R.J. Marassi, M.B.G. López, L.G. Queiroz, et al., Biochem. Eng. J. 178 (2022) 108283.
[44] Y. Wang, Y. Chen, Q. Wen, et al., Energy 189 (2019) 116342.
[45] Y.Y. Fang, B.Z. Yuan, Y.J. Jiang, et al., J. Mater. Chem. A 10 (2022) 4915–4925.
[46] L. Zhang, R. Wang, H. Li, et al., Chem. Eng. J. 500 (2024) 156807.
[47] L. Han, P.V. Chang, Curr. Opin. Chem. Biol. 76 (2023) 102351.
[48] S. Peng, J. Li, Y. Hu, et al., Small 20 (2024) 2407614.
[49] X.Q. Lin, Z.L. Li, X.Q. Chen, et al., Bioresour. Technol. 416 (2025) 131723.
[50] Y. Lu, K. Feng, C. Wu, et al., Energy Fuels 36 (2022) 514–520.
[51] Y. Gao, M. Liu, X. Zhao, et al., Ecotoxicol. Environ. Saf. 225 (2021) 112785.
[52] B. Zhang, S. Shi, R. Tang, et al., Biotechnol. Adv. 66 (2023) 108175.